

© 2019 Optical Society of America.








Users may use, reuse, and build upon the article, or use the article for text or data mining, so long as such uses are for non-commercial purposes and appropriate attribution is maintained. All other rights are reserved.

LINK TO ONLINE ABSTRACT IN THE OSA JOURNAL:

<https://opg.optica.org/boe/fulltext.cfm?uri=boe-14-11-5994&id=541182>



# Assessment of power spectral density of microvascular hemodynamics in skeletal muscles at very low and low-frequency via near-infrared diffuse optical spectroscopies

CATERINA AMENDOLA,<sup>1,\*</sup>  MAURO BUTTAFAVA,<sup>2</sup> TALYTA CARTEANO,<sup>3</sup> LETIZIA CONTINI,<sup>1</sup> LORENZO CORTESE,<sup>4</sup>  TURGUT DURDURAN,<sup>4,5</sup>  LORENZO FRABASILE,<sup>1</sup> CLAUDIA NUNZIA GUADAGNO,<sup>6</sup> U MUT KARADEINZ,<sup>4</sup> MICHELE LACERENZA,<sup>2</sup> JAUME MESQUIDA,<sup>7</sup> SHAHRZAD PARSA,<sup>8</sup> REBECCA RE,<sup>1,9</sup> DIEGO SANOJA GARCIA,<sup>3</sup> SANATHANA KONUGOLU VENKATA SEKAR,<sup>6</sup> LORENZO SPINELLI,<sup>9</sup>  ALESSANDRO TORRICELLI,<sup>1,9</sup> ALBERTO TOSI,<sup>10</sup> UDO M. WEIGEL,<sup>8</sup> M. ATIF YAQUB,<sup>4</sup>  MARTA ZANOLETTI,<sup>4</sup>  AND DAVIDE CONTINI<sup>1</sup> 

<sup>1</sup>Dipartimento di Fisica, Politecnico di Milano, Milan, Italy

<sup>2</sup>PIONIRS s.r.l., Milan, Italy

<sup>3</sup>ASPHALION S.L., Barcelona, Spain

<sup>4</sup>ICFO - Institut de Ciències Fotòniques, The Barcelona Institute of Science and Technology, Castelldefels (Barcelona), Spain

<sup>5</sup>Institució Catalana de Recerca i Estudis Avançats (ICREA), Barcelona, Spain

<sup>6</sup>BioPixS Ltd – Biophotonics Standards, IPIC, Tyndall National Institute, Lee Maltings Complex, Cork, Ireland

<sup>7</sup>Critical Care Department, Parc Taulí Hospital Universitari. Institut D'Investigació i Innovació Parc Taulí I3PT, Sabadell, Spain

<sup>8</sup>HemoPhotonics S.L., Castelldefels, (Barcelona), Spain

<sup>9</sup>Istituto di Fotonica e Nanotecnologie, Consiglio Nazionale delle Ricerche, Milano, Italy

<sup>10</sup>Politecnico di Milano, Dipartimento di Elettronica, Informazione e Bioingegneria, Milan, Italy

All authors are listed in alphabetic order except for the first and the last authors

\*[caterina.amendola@polimi.it](mailto:caterina.amendola@polimi.it)

**Abstract:** In this work, we used a hybrid time domain near-infrared spectroscopy (TD-NIRS) and diffuse correlation spectroscopy (DCS) device to retrieve hemoglobin and blood flow oscillations of skeletal muscle microvasculature. We focused on very low (VLF) and low-frequency (LF) oscillations (*i.e.*, frequency lower than 0.145 Hz), that are related to myogenic, neurogenic and endothelial activities. We measured power spectral density (PSD) of blood flow and hemoglobin concentration in four muscles (thenar eminence, plantar fascia, sternocleidomastoid and forearm) of 14 healthy volunteers to highlight possible differences in microvascular hemodynamic oscillations. We observed larger PSDs for blood flow compared to hemoglobin concentration, in particular in case of distal muscles (*i.e.*, thenar eminence and plantar fascia). Finally, we compared the PSDs measured on the thenar eminence of healthy subjects with the ones measured on a septic patient in the intensive care unit: lower power in the endothelial-dependent frequency band, and larger power in the myogenic ones were observed in the septic patient, in accordance with previous works based on laser doppler flowmetry.

© 2023 Optica Publishing Group under the terms of the [Optica Open Access Publishing Agreement](#)

## 1. Introduction

The vascular endothelium is a thin layer of cells that lines the inner surface of blood vessels throughout the entire circulatory system, from the heart to the smallest capillaries. Endothelial cells have fundamental roles for the organism as they regulate blood vessel tone, hemostasis, and fluid filtration. Several diseases, either chronic such as diabetes, or acute such as bacterial and/or viral infections can affect endothelial cell function [1,2]. Among them, septic shock is a potentially fatal medical condition in response to an infection. It causes endothelial dysfunction, that affects vasoregulation, barrier function and homeostasis, leading to tissue hypoxia, that can cause the death of the individual [1]. Several endeavors have been undertaken to develop practical, non-invasive monitoring techniques for evaluating microcirculatory performance in septic shock, ranging from tissue hypoxia at the microvascular level to endothelial function assessment. However, there remains the need for more robust, reliable and comprehensive monitoring approaches [2].

Nowadays, the most used non-invasive techniques for evaluating endothelial dysfunction are flow-mediated dilation (FMD) measured by ultrasound (US), magnetic resonance imaging (MRI), and pulse wave analysis (PWA) or pulse contour analysis (PCA) [3,4]. However, these techniques suffer from some limitations: it has been observed that FMD methods require trained experts, and it is operator dependent [5–7]; on the other side, PWA and PCA are limited by their poor reproducibility [8].

Recently, two emerging techniques have been tested in clinics, laser Doppler flowmetry (LDF) and photoplethysmography (PPG), which evaluate endothelial activities by analyzing the frequency components of blood flow and volume, respectively. From LDF and PPG studies, it has been observed that blood flow oscillations are related to different physiological processes depending on their frequency [9]: components in the range [0.6 - 2.0] Hz are related to cardiac functions; components in the range [0.145 - 0.6] Hz are related to respiratory activity; components in the range [0.052- 0.145] Hz are related to myogenic activity; components in the range [0.021 - 0.052] Hz, are related to neurogenic (sympathetic) activity; and very low frequency (VLF) components [0.0095 - 0.021] Hz are related to the endothelial activity dependent on nitric oxide (NO). The cardiac and respiratory components are centrally mediated by heart and lungs, respectively; whereas the low frequency (LF, < 0.145 Hz) and VLF activities (<0.021 Hz) originate locally, as a response to the vessel's tone regulation. In particular, myogenic activities are microvascular contraction and relaxation in response to changes in blood pressure; whereas neurogenic activities are variations of blood vessel diameters in response to local stimuli of the nervous system. On the other hand, NO is a vasodilator, that can be released by endothelial cells, causing spontaneous variations in the vascular tone. Dysfunctions of endothelium activity have been observed to be related to the loss of the protective role of NO (the endothelium-derived relaxing factors). Thus, VLF oscillations of blood flow, are associated with spontaneous NO-related endothelial activities, needed for the regulation of blood flow, pressure and vascular tone [10–15].

However, LDF and PPG techniques suffer from some drawbacks. LDF measures only relative variations in the blood flux of the skin, and it is commonly considered poorly reproducible [16]; whereas PPG assesses blood volume in peripheral arteries, which might not reflect tissue hemodynamics [17,18]. Thus, a technique that overcomes these drawbacks is necessary to monitor the progression of diseases affecting endothelial function [19].

Recently, continuous wave near-infrared spectroscopy (CW-NIRS) has been tested in the clinical environment to retrieve the endothelial health in several critical care settings, mostly those involving severe infections, and ranging from severe cardiovascular impairment, as in septic shock, to acute respiratory distress syndrome (ARDS) [20,22–26]. In these studies, the authors performed NIRS measurements on peripheral muscles during a vascular occlusion tests (VOT), which consists of a short period of induced ischemia in the muscle [27]. The choice of

monitoring peripheral muscles is motivated by the fact that they are non-privileged organs with poor compensatory mechanisms, showing hemodynamic alterations in advance than vital organs (additionally, these measuring sites are easily accessible for VOT) [28]. They demonstrated that NIRS combined with VOT allows retrieving hemodynamic parameters related to endothelial health and microvascular reactivity (*e.g.*, reoxygenation rate and hyperemic response after the occlusion period) which are associated with patients' outcomes, from the severity of lung involvement in ARDS to the evolution of organ failure and mortality, paving the way for the use of NIRS techniques for monitoring endothelial function. However, CW-NIRS suffer from some limitations, it suffers from motion artifacts [29], it is affected by skin pigmentation [30], and more in general by superficial tissues. In the VASCOVID project [31] (funded by the Horizon Europe 2020 program), some of those limitations have been overcome by exploiting more complex techniques: time domain NIRS (TD-NIRS) [32] and diffuse correlation spectroscopy (DCS) [33].

In the framework of the VASCOVID project, we explored a different methods for assessing microvasculature function, which exploits non-invasive and stationary diffuse optical (DO) monitoring of peripheral muscles with no need for any other subsidiary and/or discomfort intervention (*i.e.*, VOT). Starting from the knowledge gained from LDF and PPG literature, we tested the possibility to evaluate endothelial and more in general microvascular functions by analyzing the frequency spectrum of hemodynamic and microcirculatory parameters measured by a DO device [34]. We used a hybrid time domain NIRS (TD-NIRS) [32] and diffuse correlation spectroscopy (DCS) [33] instrument to assess power spectral density of hemodynamic parameters in skeletal muscle microvasculature during a rest condition. TD-NIRS module allows to assess hemoglobin concentration (oxygenated hemoglobin, HbO<sub>2</sub>; deoxygenated hemoglobin, HHb; total hemoglobin, tHb) and tissue oxygen saturation S<sub>t</sub>O<sub>2</sub>, whereas DCS gives information on blood flow through the blood flow index (BFI). Compared to VOT, the frequency analysis of the hemodynamic signals acquired during rest allows to evaluate the mechanisms underlying microvascular function (*i.e.*, myogenic, neurogenic and endothelial-spontaneous oscillations) giving a wider description of microvascular health.

Recently, few studies have been published exploiting NIRS to measure LF (<0.145 Hz) and VLF (<0.021 Hz) oscillations to investigate cerebral autoregulation [35–37] and to study post-exercise muscles oxygenation [38–41]. However, to our knowledge, no studies have been conducted combining TD-NIRS and DCS to study skeletal muscles' oxygen saturation and blood flow LF and VLF oscillations during rest.

In this work, we aimed to demonstrate the detectability of oscillations, *i.e.*, frequency peaks, that are related to microvascular and endothelium functions (myogenic, neurogenic activities, and endothelium-spontaneous activities) through frequency analysis of hybrid DO measurements. We focused on LF and VLF oscillations, and we investigated four different body districts: thenar eminence, plantar fascia, sternocleidomastoid and forearm muscles (wrist flexor group). We selected these muscles to understand whether oscillations in DO measurements could be influenced by the proximity of large vessels (such as the sternocleidomastoid artery), as well as to determine if these oscillations are more pronounced in particular muscles, such as the distal muscles of thenar eminence and plantar fascia. Moreover, the results obtained for healthy subjects were compared with measurements performed on a septic patient in the intensive care unit (ICU).

## 2. Materials and methods

### 2.1. Protocol on healthy volunteers

The experiment was conducted under the declaration of Helsinki, all subjects cooperated voluntarily and previously provided written informed consent to the procedures of the study, which was approved by the Ethics Committee of Politecnico di Milano (authorization n. 037/2020).

For each volunteer, hemodynamic parameters of thenar eminence, plantar fascia, sternocleidomastoid and forearm muscles were monitored sequentially (a schematic of the probe position is reported in Fig. 1) with a randomized order. The measurements were performed during rest, and they lasted 15 minutes for each probe position.

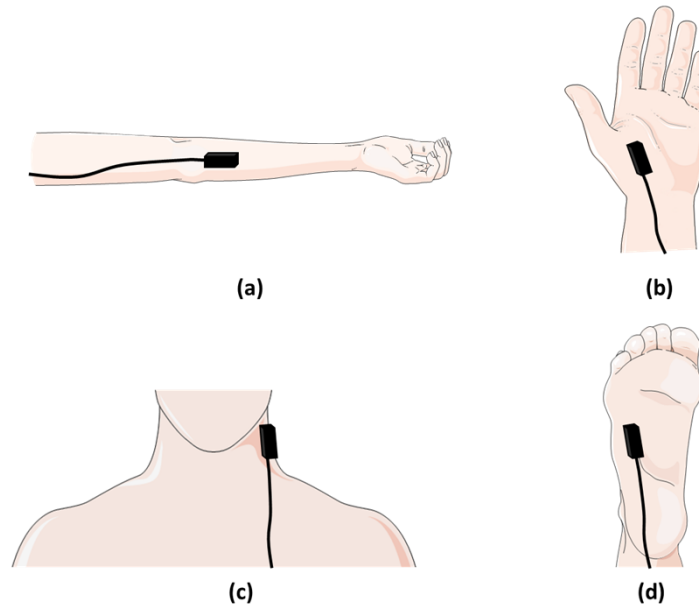


**Fig. 1.** Schematic of the probe position during measurements: panel a) forearm, panel b) thenar eminence, panel c) sternocleidomastoid, d) plantar fascia.

During the measurements, subjects were lying on a bed, in a semirecumbent position (with backrest tilted  $45^\circ$  upward). Before DO measurements, height and weight of the participants were collected, their systolic and diastolic pressure were acquired and the depth of the primary muscle to be probed (distance of the muscle upper surface from skin) was measured via ultrasound (SonoScape Medical Corp., China).

### 2.2. Protocol for septic patient

Finally, we performed a resting state measurement on the thenar eminence of an ICU septic patient at Hospital Parc Taulí (Sabadell, Barcelona). Ethical approval for this study was provided by the Comitè d'Ètica i Investigació amb Medicaments of the Institut d'Investigació i Innovació Parc Taulí (I3PT).

The hemodynamic parameters were measured during resting state for 500 s instead of the 900 s (time length used for healthy subjects) and only on the thenar eminence (easily accessible muscles in ICU patients), due to the need to reduce impact with the clinical routine of the patient.

### 2.3. TD-NIRS and DCS devices

The device used in the protocol for healthy volunteers was a hybrid TD-NIRS and DCS device previously developed in Politecnico di Milano [34]. The device allows simultaneous measurements of hemoglobin concentration and blood flow with an acquisition rate of 0.8 Hz. The TD-NIRS module consists of two pulsed diode lasers operating at 670 nm and 830 nm, with a repetition rate of 50 MHz. The photons backscattered by the tissues are collected by a single photon detector and the integrated electronic board allows to reconstruct the pulse reemitted by the tissue with a resolution of 10 ps [42]. The DCS module uses a highly coherent continuous-wave

laser source at 785 nm. To increase the signal to noise ratio of the DCS signal [43], a bundle of four single mode fibers was used to collect backscattered light, which drives the photons to four single-photon avalanche diodes. Finally, the intensity autocorrelation function is reconstructed by a 4-channel hardware correlator (for further detail on the device see [34]). The interfiber distances were set to 1.5 cm for the DCS module and 2 cm for the TD-NIRS module as a tradeoff among the smallest muscle dimension, signal-to-noise-ratio, and validity of diffusion theory. The optical probe was 3D printed with a flexible filament to better adapt to tissue surface curvature, and hosts 3 mm prisms which deflect the light by 90° [44]. This setup allows measurements in the so-called “reflectance geometry” with optical fibers parallel to the sample leading to a more comfortable setting (see Fig. 1).

DO measurement on a septic patient was performed with the VASCOVID device [45], a hybrid TD-NIRS and DCS device, with an acquisition frequency of 1 Hz. Compared to the set-up used to perform the measurements on healthy volunteers, the VASCOVID probe has an inter-fiber distance of 2.5 cm for both TD-NIRS and DCS modules.

#### 2.4. Data preprocessing

TD-NIRS data were analyzed with the semi-infinite homogeneous model for photon diffusion in the reflectance geometry [46] under the partial current boundary conditions (PCBC) [47]: absorption ( $\mu_a$ ) and reduced scattering coefficients ( $\mu_s'$ ) at 670 nm and 830 nm were retrieved with a Levenberg-Marquardt minimization algorithm [48], exploiting an in-house developed software, based on C language. Then, by means of the Beer's law, hemoglobin concentration was computed from  $\mu_a$  assuming that HbO<sub>2</sub> and HHb were the two chromophores mainly contributing to the tissue absorption at the measured wavelengths.

BFI was calculated from DCS data at 785 nm, using the diffusion equation of electric field autocorrelation function for semi-infinite homogeneous medium [49,50]. A code written in Matlab was used to find the BFI value that minimizes, utilizing the Nelder-Mead simplex non-linear method, the difference between the derived electric field autocorrelation function and the theoretical model [51]. In the DCS fitting procedure, absorption and reduced scattering coefficients retrieved by TD-NIRS measurements at 830 nm were used as input parameters approximating the optical properties at 785 nm.

The optical and hemodynamic parameters measured during 15 min of resting state were averaged for each volunteer and probed muscle. Then, for each body position the means among all the participants were calculated for optical and hemodynamic parameters. The body mass index (BMI) was computed from the height and weight of each participant.

To compare time traces measured in different body positions, we removed baseline shifts and considered relative variation of the hemodynamic parameters. Thus, the following steps were followed: each HHb, HbO<sub>2</sub>, tHb, S<sub>t</sub>O<sub>2</sub> and BFI time course was normalized by the 3<sup>rd</sup> order polynomial that best fit the data; then to remove the continuous component, the normalized data were detrended as suggested in previous studies [35,52,53].

#### 2.5. Frequency domain analysis

For each subject and probe position, the power spectral density (PSD) was computed by means of the Welch algorithm, with Hamming windows of 300 seconds, with an overlap of 50%. Finally, for each position, we computed the average PSD and standard error at each frequency among all the volunteers for all the hemodynamic parameters.

To evaluate changes among the PSDs of different muscles, we selected three frequency intervals [9]: I<sub>1</sub> = [0.0095; 0.021] Hz; I<sub>2</sub> = [0.021; 0.052] Hz; I<sub>3</sub> = [0.052; 0.145] Hz, the first corresponding to the VLF (NO-dependent endothelial activity), the second to LF neurogenic activity, the third to LF myogenic activity. For these intervals, we computed the absolute and relative (*i.e.*, with respect to the total area of the spectrum) spectrum area: absolute area gives information on



the power of the spectral component (*e.g.*, myogenic, neurogenic or endothelial) in the signal, whereas the relative area gives insight on the relative weight the different spectral components have in PSD.

Finally, the HHb, HbO<sub>2</sub>, tHb, S<sub>t</sub>O<sub>2</sub> and BFI spectra retrieved for the ICU patient were qualitatively compared with the ones measured on the thenar eminence of healthy volunteers.

## 2.6. Statistical analysis

The results obtained for the time courses and PSD were analyzed to evaluate statistically significant differences and correlations.

Concerning the time courses of tHb and S<sub>t</sub>O<sub>2</sub> we studied the correlations with BMI and the probed muscle depth using the Pearson correlation coefficient (R). Correlations were considered statistically significant for p-value < 0.05. The average optical and hemodynamic parameters among different subjects was calculated, and the standard deviation was computed to quantify intersubject variability.

In case of frequency analysis, we computed the average of PSDs among different subjects and we showed their standard error, to compare the mean of different PSDs and highlight the uncertainty around them due to the low number of subjects.

For the comparison of PSD in different body compartments, we performed the Wilcoxon signed-rank test on the absolute and relative areas computed for the three frequency intervals of interest (I<sub>1</sub> = [0.0095; 0.021] Hz; I<sub>2</sub> = [0.021; 0.052] Hz; I<sub>3</sub> = [0.052; 0.145]). The Bonferroni correction was performed to account for the multiple comparisons.

## 3. Results and discussion

### 3.1. Mean physiological, demographic and hemodynamic parameters

Fourteen healthy volunteers (4 females and 10 males) were recruited in this study. In Table 1 we report the average (and interquartile range, IQR) values of systolic/diastolic pressure, BMI, and the age of the participants at the moment of the measurements.

**Table 1. Average and interquartile range (IQR) of age, body mass index (BMI), systolic and diastolic pressure of the healthy participants at the moment of the measurement.**

	All subjects (N = 14)		Female (N = 4)		Male (N = 10)	
	Average	IQR	Average	IQR	Average	IQR
Diastolic pressure (mmHg)	71.5	10.5	68	12	72.9	14.7
Systolic pressure (mmHg)	115.8	13	107	14.25	119	10.0
BMI (kg/m <sup>2</sup> )	21.9	2.5	20.55	1.97	22.44	1.96
Age (years)	27.2	4.5	28.25	4.25	26.8	4.5

Average values of muscles depth and of the DO related parameters are reported in Table 2, for all the locations measured. Muscle depth shows very low thicknesses of the overlaying tissues, always lower than 5 mm (in all the subjects and probed areas).

Correlations between the hemodynamic parameters and participants' age and pressure were studied, but no correlation was found (p-value > 0.05). Moreover, no correlation was observed between hemodynamic parameters and muscle depth, neither between hemodynamic parameters and BMI (data not shown).

**Table 2. Average and standard deviation (std) of anatomical, optical, and hemodynamic parameters during resting state measurements in four body positions, divided according to the participant sex.**

		Thenar eminence		Forearm		Sternocleidomastoid		Plantar fascia	
		Mean	std	Mean	std	Mean	std	Mean	std
All subjects	Muscle depth (mm)	2.3	0.22	3.11	1.01	2.78	0.77	0.94	0.63
	$\mu_{a,670}$ (cm <sup>-1</sup> )	0.38	0.08	0.32	0.07	0.28	0.07	0.14	0.08
	$\mu_{a,830}$ (cm <sup>-1</sup> )	0.26	0.06	0.29	0.07	0.26	0.07	0.12	0.05
	$\mu'_{s,670}$ (cm <sup>-1</sup> )	7.30	1.3	9.01	1.1	10.61	1.53	11.96	1.4
	$\mu'_{s,830}$ (cm <sup>-1</sup> )	5.22	1.1	7.26	1.30	8.85	1.63	11.01	1.64
	tHb (μM)	128.45	29.53	140.22	31.77	127.1	32.73	56.33	22.49
	S <sub>t</sub> O <sub>2</sub> (%)	59.90	6.03	72.68	2.76	73.02	4.18	69.88	3.75
	BFI (10 <sup>-9</sup> cm <sup>2</sup> /s)	18.3	9.03	7.34	3.5	28.0	20.0	0.83	0.35
Female	Muscle depth (mm)	2.42	0.34	3.83	0.89	3.4	0.36	0.91	0.10
	$\mu_{a,670}$ (cm <sup>-1</sup> )	0.37	0.13	0.24	0.04	0.25	0.05	0.14	0.04
	$\mu_{a,830}$ (cm <sup>-1</sup> )	0.22	0.06	0.23	0.03	0.22	0.02	0.11	0.02
	$\mu'_{s,670}$ (cm <sup>-1</sup> )	6.61	1.3	8.92	0.55	10.71	1.66	11.48	0.91
	$\mu'_{s,830}$ (cm <sup>-1</sup> )	4.5	0.41	6.14	0.35	9.21	2.33	10.57	1.06
	tHb (μM)	112.99	32.20	110.47	14.30	106.80	10.64	53.46	12.46
	S <sub>t</sub> O <sub>2</sub> (%)	54.39	9.50	73.74	1.98	72.21	4.68	67.54	3.30
	BFI (10 <sup>-9</sup> cm <sup>2</sup> /s)	10.7	3.8	6.11	3.77	29.8	28.5	0.68	0.11
Male	Muscle depth (mm)	2.24	0.28	2.83	0.90	2.54	0.83	0.96	0.74
	$\mu_{a,670}$ (cm <sup>-1</sup> )	0.38	0.06	0.35	0.07	0.30	0.08	0.14	0.06
	$\mu_{a,830}$ (cm <sup>-1</sup> )	0.27	0.05	0.31	0.06	0.28	0.07	0.12	0.05
	$\mu'_{s,670}$ (cm <sup>-1</sup> )	7.57	1.04	9.04	1.22	10.56	1.6	12.14	1.45
	$\mu'_{s,830}$ (cm <sup>-1</sup> )	5.52	1.02	7.71	1.45	8.71	1.31	11.19	1.73
	tHb (μM)	134.63	24.18	152.11	31.43	135.22	33.46	57.47	24.35
	S <sub>t</sub> O <sub>2</sub> (%)	62.10	5.87	72.25	2.84	73.33	4.25	70.81	3.90
	BFI (10 <sup>-9</sup> cm <sup>2</sup> /s)	21.3	9.33	7.83	3.4	27.2	15.8	0.89	0.38

### 3.2. Time and frequency analysis

In Fig. 2, we report percentage variations of tHb, S<sub>t</sub>O<sub>2</sub> and BFI for one exemplary volunteer when the probe was placed on the thenar eminence (first row), forearm (second row), sternocleidomastoid (third row) and on the plantar fascia (fourth row); similar results were obtained for the other participants. HHb, HbO<sub>2</sub> (data not shown), tHb, S<sub>t</sub>O<sub>2</sub> (left column), do not show significant differences between the four positions, and the percentage variations are negligible. Concerning BFI (right column), strong differences can be observed between the data measured on the arm and



**Table 3. Systolic/diastolic pressure, BMI, age, and average optical and hemodynamic parameters ( $\pm$  their standard deviations) over the 500s acquisition measured on the thenar eminence of the ICU septic patient, at the moment of the enrollment.**

Diastolic pressure (mmHg)	55
Systolic pressure (mmHg)	119
BMI (kg/m <sup>2</sup> )	30.6
Age (years)	61
$\mu_{a,685}$ (cm <sup>-1</sup> )	0.20 $\pm$ 0.002
$\mu_{a,830}$ (cm <sup>-1</sup> )	0.17 $\pm$ 0.002
$\mu'_{s,685}$ (cm <sup>-1</sup> )	8.03 $\pm$ 0.11
$\mu'_{s,830}$ (cm <sup>-1</sup> )	6.94 $\pm$ 0.10
tHb ( $\mu$ M)	86.3 $\pm$ 1.39
S <sub>t</sub> O <sub>2</sub> (%)	60.25 $\pm$ 1.05
BFI (10 <sup>-9</sup> cm <sup>2</sup> /s)	15.1 $\pm$ 4.55

sternocleidomastoid with respect to the thenar eminence and plantar fascia: large oscillations of about 100% (50%) are observed when the probe was positioned on the thenar eminence (plantar fascia) compared to the arm and sternocleidomastoid.

Starting from the time traces, following the steps reported in Sec. 2.4, the PSDs of all hemodynamic parameters were reconstructed for each participant and muscle measured. The average PSDs of hemodynamic parameters and BFI within all the participants are reported in Fig. 3 and Fig. 4 respectively, where lines represent the average among all the subjects and shadows are the corresponding standard errors. The PSDs for HHb (Fig. 3(a)), HbO<sub>2</sub> (Fig. 3 panel (b)), tHb (Fig. 3 panel (c)) and S<sub>t</sub>O<sub>2</sub> (Fig. 3(e)) have very small amplitude (as expected from the small percentage variations reported in Fig. 2), however some peaks at LF and VLF can be distinguished. Larger PSDs were retrieved for BFI, about 2 orders of magnitude with respect to the hemodynamic parameters (see Fig. 4). Clear differences can be observed in PSDs of BFI (Fig. 4) where thenar eminence (blue line) or plantar fascia (red line) results are compared with the ones of forearm (black line) or sternocleidomastoid (green line).

The absolute and relative areas of PSD at three intervals,  $I_1 = [0.0095; 0.021]$  Hz,  $I_2 = [0.021; 0.052]$  Hz, and  $I_3 = [0.052; 0.145]$  Hz were computed, and statistical analysis was performed following the procedure reported in Sec. 2.5 and Sec. 2.6. Concerning BFI (Appendix A, Table 4) we observed a statistically significant difference in absolute PSD areas ( $p < 0.0086$ ) between the two distal muscles (thenar eminence and plantar fascia) with respect to the less distal muscles (forearm and sternocleidomastoid). No significant differences were observed in the relative areas of the BFI PSDs. For the sake of completeness, statistical analysis was performed also on hemoglobin concentrations and S<sub>t</sub>O<sub>2</sub> parameters. Results from the statistical analysis performed on absolute and relative areas are reported in Appendix A (Table 5 for HHb, Table 6 for HbO<sub>2</sub>, Table 7 for tHb and Table 8 for S<sub>t</sub>O<sub>2</sub>). Statistically significant differences vary among different hemodynamic parameters, spectral intervals, and between relative and absolute areas.

### 3.3. ICU septic patient: a case study

In Table 3, we report the values of systolic/diastolic pressure, BMI, age, optical and hemodynamic parameters measured on the thenar eminence of the ICU septic patient, at the moment of the enrollment. The measurements were performed on his sixth day of admission at ICU, where the patient was mechanically ventilated and was receiving low doses of vasopressors.

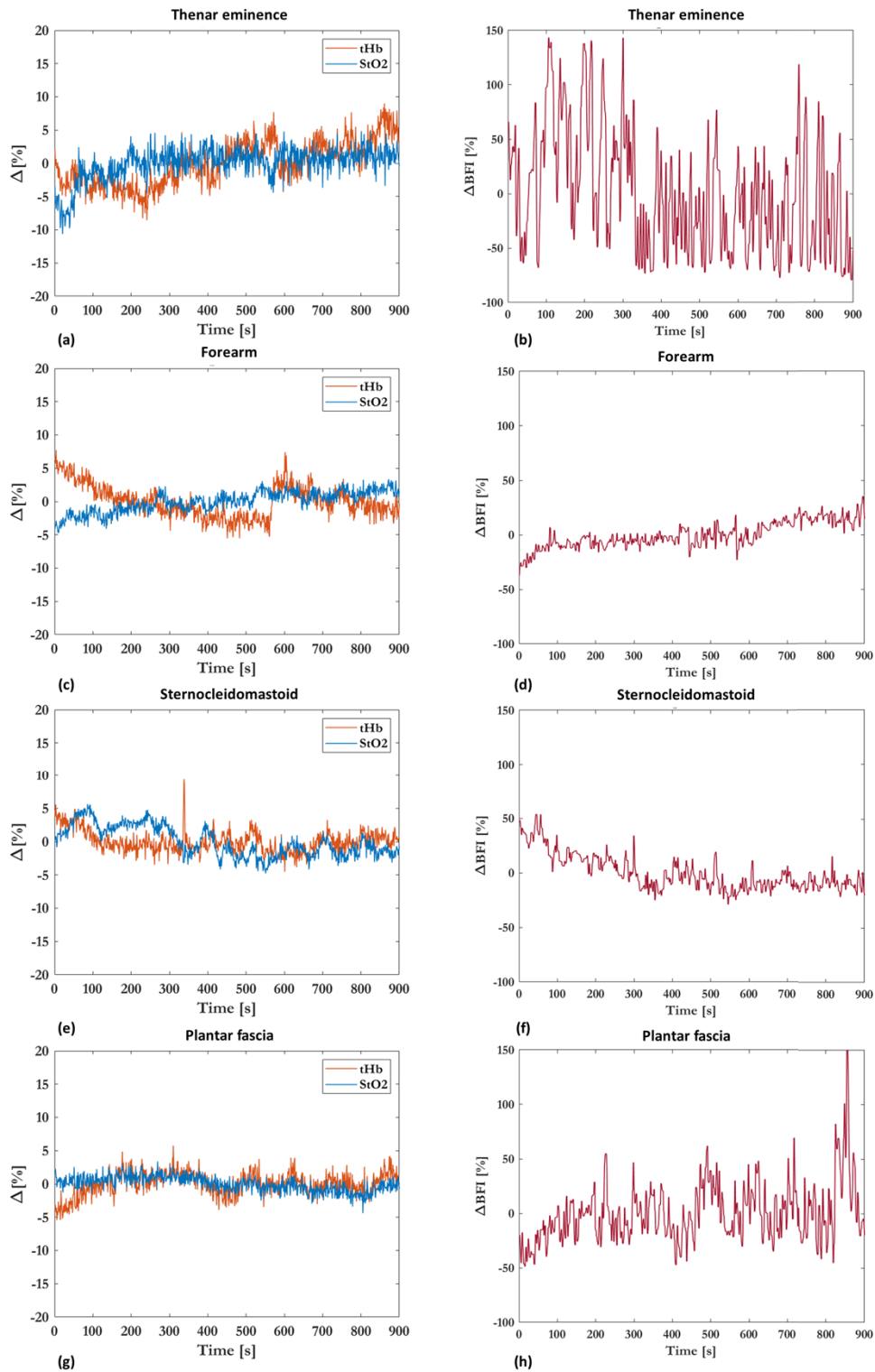


**Fig. 2.** Time traces of percentage variations of tHb, S<sub>t</sub>O<sub>2</sub> (left column) and BFI (right column) measured on thenar eminence (panels (a) and (b)), forearm (panels (c) and (d)), sternocleidomastoid (panels (e) and (f)) and plantar fascia (panels (g) and (h)) of one exemplary healthy volunteer.

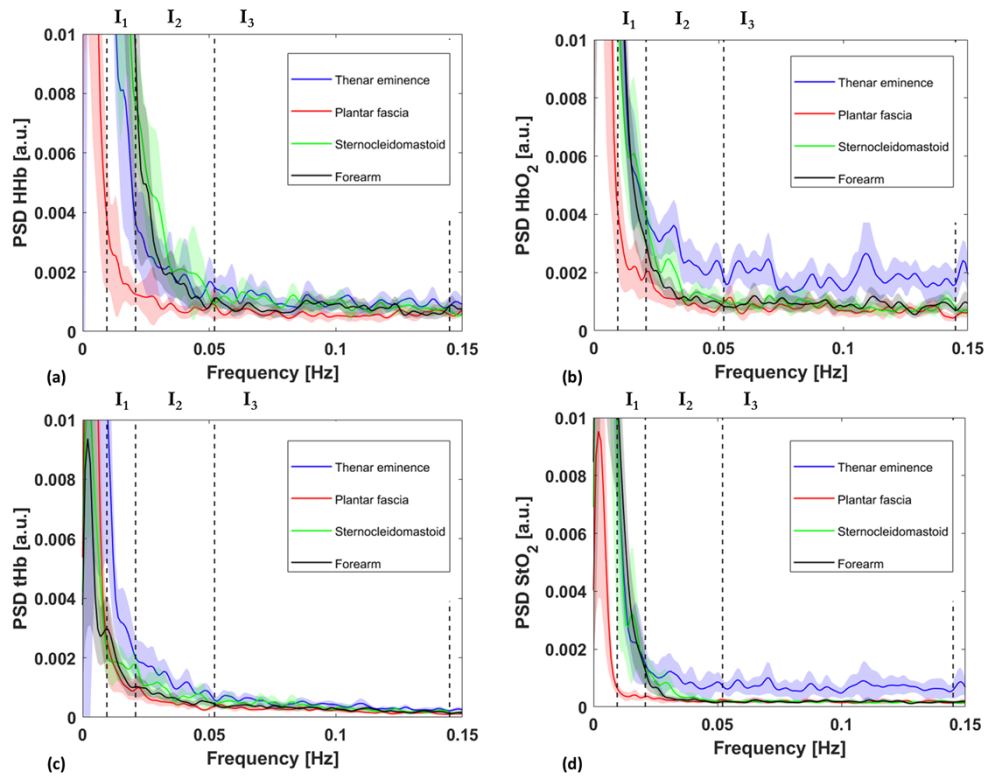


**Fig. 3.** Zoom of the power spectral density (PSD) highlighting the spectral components at the three intervals of deoxygenated hemoglobin (HHb, panel (a)), oxygenated hemoglobin ( $\text{HbO}_2$ , panel (b)), total hemoglobin (tHb, panel (c)), tissue oxygen saturation ( $\text{StO}_2$ , panel (d)), averaged among all the participants, in different muscles. Lines are the average values, while shadows are the corresponding standard errors.

In Fig. 5 and Fig. 6, we report the PSD obtained for hemodynamic parameters and BFI, respectively, measured on the thenar eminence of the septic patient (yellow line), and of healthy volunteers (blue line). For all the variables, the behavior of PSDs shows differences at VLF ( $<0.021$  Hz), suggesting that spontaneous endothelial activities might be different in the septic patient compared to healthy subjects. In Fig. 7, the absolute (left column) and relative (right column) areas of PSDs in the three spectrum intervals computed for the septic patient are reported as red diamond and compared to the ones measured for healthy volunteers. In the  $I_1$  interval at VLF (component related to NO-dependent endothelium activities), the absolute and relative area of the septic patient is lower than the 25<sup>th</sup> percentile computed for healthy volunteers for all the hemodynamic parameters. In the third interval  $I_3$  (related to myogenic activity) the relative area measured for the septic patient is higher than the 75<sup>th</sup> percentile computed for healthy volunteers. In Appendix B (Table 9), we reported the median values and IRQ of PSD areas of hemodynamic parameters measured on healthy volunteers and on the septic patient, in the thenar eminence.

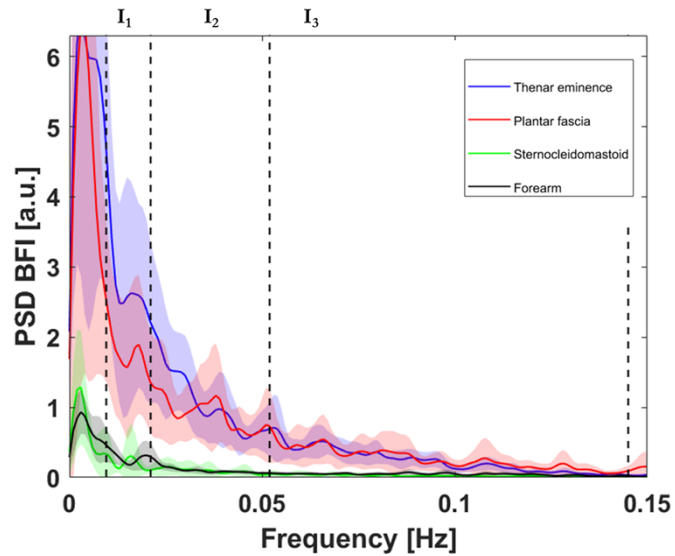


**Fig. 4.** Power spectral density (PSD) of blood flow index (BFI) averaged among all the participants, in different muscles. Lines are the average values, while shadows are the corresponding standard errors.

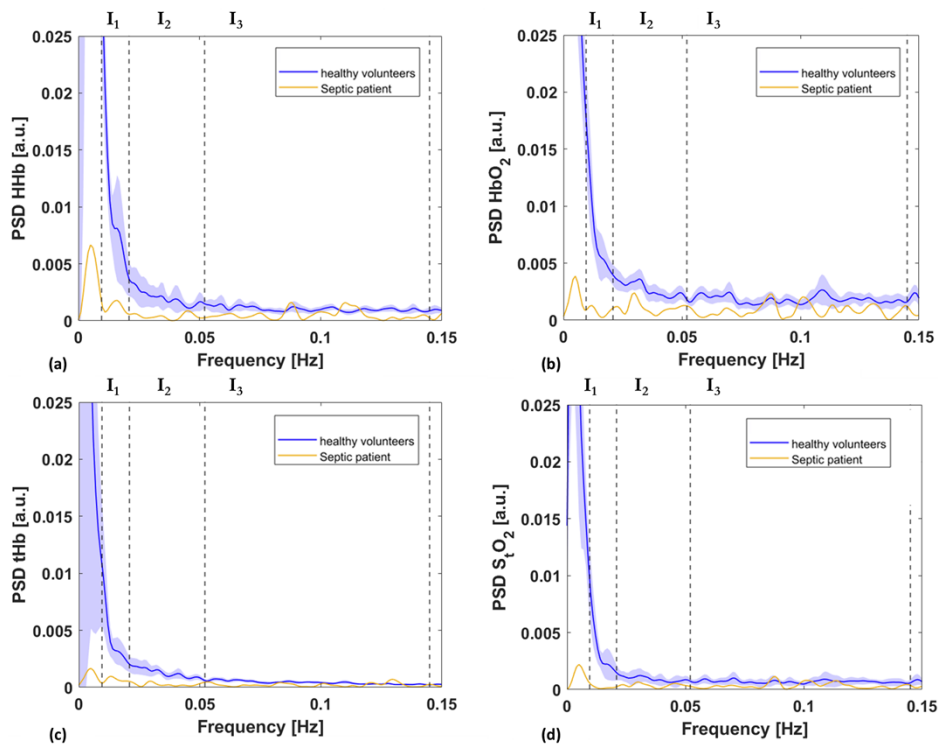


**Fig. 5.** Power spectral density (PSD) of HHb (panel (a)), HbO<sub>2</sub> (panel (b)), tHb (panel (c)) and S<sub>t</sub>O<sub>2</sub> (panel (d)) averaged among all the volunteers (blue line) compared with PSDs measured for the septic patient (yellow line), on the thenar eminence.

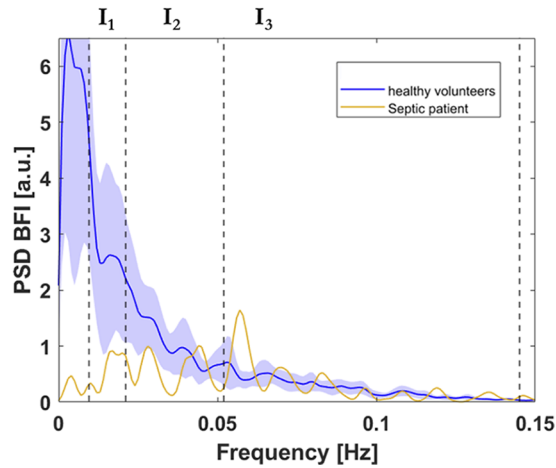


**Fig. 6.** Power spectral density (PSD) of blood flow index (BFI) averaged among all the volunteers (blue line) compared with PSD of BFI measured on a septic patient (yellow line), on the thenar eminence.

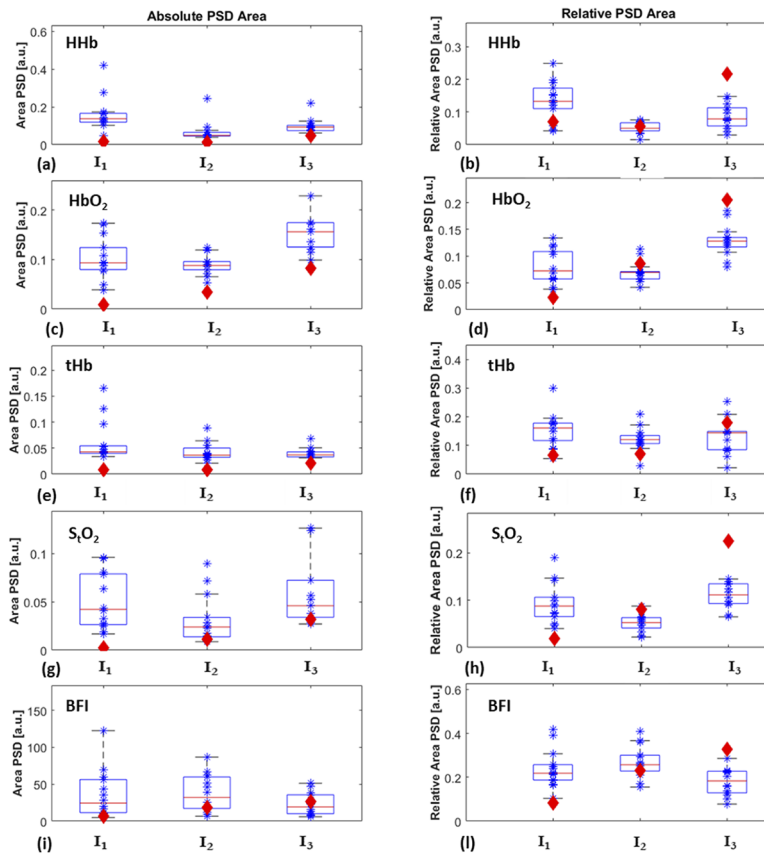


**Fig. 7.** Box plot of absolute and relative areas of PSDs measured on the thenar eminence computed in the three intervals of interest in case of healthy subjects (asterisk), compared to the ones measured in the septic patients (red diamond). The red lines inside the boxes represent the median, the bottom and top edges of the box indicate the 25<sup>th</sup> and 75<sup>th</sup> percentiles, for healthy volunteers. The whiskers extend to the most extreme data points not considered outliers.

#### 4. Discussion

In this work, we explored the possibility to obtain insights into the microvascular and endothelial health of human subjects, by studying LF and VLF oscillations at rest in skeletal muscles hemodynamic parameters measured by TD-NIRS and DCS. NIRS has already been successfully used to evaluate endothelial health of several populations of critical care patients [20–24,26,54,55]. However, in the previous literature NIRS measurements on peripheral muscles were combined with VOT, evaluating the endothelial function from the re-oxygenation rate and hyperemic peak or area measured at the end of the occlusion [21,23–25]. The main advantage of the approach reported in this paper is the potential to retrieve information related to microvascular and endothelial function by measuring hemodynamic parameters and BFI in resting state condition, avoiding subsidiary intervention as VOT. Furthermore, VOT-derived variables cannot be isolated from global upstream hemodynamic parameters, such as blood pressure.

Here, the hemodynamic resting state of four muscles was studied: thenar eminence and plantar fascia as distal muscles, sternocleidomastoid to highlight whether DO measurements could be influenced by the proximity of large vessels, and the forearm which is generally studied in VOT works [22]. The study is limited to 14 healthy volunteers, which was sufficiently large to observe significant differences among different body positions. However, further studies including larger number of participants might be beneficial to define normal values of PSD, as suggested by diverse values obtained for median and average PSDs among the subjects. Moreover, larger population might be exploited to study possible differences between the sex and the age of the participants. Indeed, it should be noted that the septic patient is significantly older than healthy volunteers, thus a more extended and detailed study might be beneficial.

In the four distinct locations measured, all hemodynamic parameters showed VLF and LF oscillations within the range of 0.0095 and 0.145 Hz. However, BFI oscillations were observed to be significantly higher (more than 2 order of magnitude) compared to the other hemodynamic parameters (Fig. 3 and Fig. 4). Oscillations of blood flow and volume at VLF have been already observed in literature exploiting different techniques such as LDF and PPG [56], respectively. However, LDF is sensitive to superficial tissues (few millimeters), thus only to oscillations in cutaneous and adipose tissues, and PPG investigates arterial blood volume, and does not directly evaluate microvasculature. Previous works studying blood flow oscillations in peripheral (*i.e.*, fingers) skin by PPG and LDF, demonstrated that such oscillations are related to spontaneous NO-mediated endothelial activities within 0.0095-0.021 Hz [11,57–59] and to neurogenic factors in the range of 0.021-0.05 Hz [60,61]. For instance, Stefanovska et al. [59] observed significant differences in blood flow PSDs (in the range of 0.095- 0.021 Hz) between endothelium-dependent and endothelium-independent vasodilators, suggesting that endothelial activity is a rhythmic process that contributes to oscillations in blood flow with a characteristic frequency of around 0.01 Hz. After a few years, Kvandal et al. [58] studied the effect of NO and [62] prostaglandins (PGs) inhibition on blood flow oscillations. Indeed, NO and PGs are responsible for the regulation of vascular tone and blood flow. They demonstrated that the spontaneous oscillations observed in 0.0095-0.021 Hz range are mediated by NO, and they are not affected by PGs. Thus, the peaks we observed in PSD of BFI (Fig. 3 c) at VLF could be related to spontaneous NO-mediated endothelial activities.

Concerning oscillations in the range 0.021-0.052 Hz are associated to neurogenic activity [63]. In 2003 Söderström et al. [64] studied blood flow measured by LDF in skin deprived of sympathetic nerve activity and intact skin. They observed a lower blood flow normalized spectral power in the range 0.0095-0.052 Hz when the sympathetic nervous system was inhibited. Since the endothelial-dependent oscillation frequency is in the range of 0.0095-0.021 Hz, they concluded that the nervous activities in micro-vessels are observed in blood flow oscillation around 0.021-0.052 Hz.



Finally, oscillations observed in the range of 0.052- 0.145 Hz, they might be related to myogenic activities [9]. From previous literature we know that myogenic activities are triggered by variations in luminal pressure, and they regulate the internal diameter of arteries and arterioles, causing vessels constriction when blood pressure increases and dilation when it decreases [65]. Landsverk et al. [66] demonstrated that these oscillations are not related to respiratory activities neither to sympathetic nervous system, and, even though the process leading to vasoconstriction in this frequency band was largely studied, it remains unclear if the cause is vessels wall strain or stress [67]. In 1991, Falcone et al. [68] demonstrated that myogenic activities are not mediated by endothelium. Indeed, they studied in-vitro arterioles generating variations in blood pressure, and by physically removing endothelium they did not observe significant differences in response to changes of blood pressure.

Comparing the PSD computed in different muscles, the BFI VLF and LF oscillations were significantly higher in distal muscles, such as thenar eminence and plantar fascia, compared to non-distal muscles (forearm and sternocleidomastoid), suggesting that more distal regions could be more suitable to identify new biomarkers for endothelium dysfunction. Previous studies have been conducted using PPG in different body districts [69], fingers, ear lobe, etc., but PPG investigates blood volumes variations, which might behave differently from microvasculature of skeletal muscles. On the other hand, LDF has been performed on forearm, but it is sensitive only to skin blood flow, and not to muscle microvasculature. A technology similar to DCS, diffuse speckle contrast analysis (DSCA) has been recently used by Yeo et al. [41] to study VLF and LF oscillations of blood flow in four different foot positions to validate the foot angiosome concept. The authors were able to demonstrate the ability of DSCA to evaluate variations in VLF and LF blood flow oscillations due to occlusion protocols. Compared to Yeo et al., we investigated four different skeletal muscles in resting state to evaluate the optimal probe position when exploiting DCS and TD-NIRS for LF and VLF analysis of endothelial function.

Concerning HHb, HbO<sub>2</sub>, tHb and S<sub>t</sub>O<sub>2</sub>, previous studies performed using continuous wave NIRS (CW-NIRS) devices demonstrate the possibility to observe VLF and LF oscillations in  $\Delta$ Hb and S<sub>t</sub>O<sub>2</sub> after muscles exercises [38,70]. However, little is known about resting state spectra of skeletal muscles. In this work, HHb, HbO<sub>2</sub>, tHb and S<sub>t</sub>O<sub>2</sub> LF and VLF oscillations of skeletal muscles at resting state were observed, but their PSDs both in terms of absolute (more than two order of magnitude) and relative (more than half) area are significantly lower compared to the one of BFI, suggesting that BFI is more sensitive to spontaneous tone modulation of blood vessels than TD-NIRS signal. Significant differences between the four measured muscles were observed, however they vary among different hemodynamic parameters, spectral intervals, and between relative and absolute areas causing a difficult identification of a unique biomarker and suggesting that further work is needed to gain a better understanding of the usability of hemoglobin concentration and tissue oxygenation PSDs.

Finally, we compared the results of healthy subjects with the ones of an ICU septic patient whose endothelial functions is expected to be impaired (Sec. 3.3). The PSDs of HHb, HbO<sub>2</sub>, tHb, S<sub>t</sub>O<sub>2</sub> and BFI measured on the thenar eminence of the septic patient show different behavior at VLF and LF. In particular, the relative area of the PSDs of all hemodynamic parameters (Fig. 7) is lower than the 25<sup>th</sup> percentile measured on healthy subjects at frequencies < 0.021 Hz, suggesting that the endothelial activities might behave differently compared to the ones of healthy volunteers. On the other hand, the myogenic component in the PSD of the septic patient shows a larger contribution compared to the one of healthy subjects. This exemplary case is in accordance with a previous study, where LDF was used to assess endothelial health of septic patients [71], demonstrating that myogenic oscillations are enhanced in septic patients which showed a marked increase in the fraction of total power in the 0.1–0.15 Hz frequency band. The case study here reported is promising in light of the potential application of the described method to monitor endothelial impairments in septic patients in resting state conditions. It is indeed well known

that the microvascular endothelium is damaged in case of sepsis, reducing its barrier role and increasing its permeability [72,73], and such impairment is often related to patient outcome. To test this hypothesis, PSDs of a larger set of ICU septic patients will need to be measured. Indeed, the case study here reported might be affected by the sensitivity to muscle tissue in ICU patient compared to measurements on healthy volunteers. Very often, ICU patients are affected by edema, which might affect diffuse optical measurements, and the BMI of the septic patient was larger compared to the ones of healthy volunteers. However, the effects of these two factors are reduced by the low intersubject variability of superficial thickness in thenar eminence [74], and the larger interfiber distance of the VASCOVID device (2.5 cm for both TD-NIRS and DCS modules) compared to the one used to measure healthy volunteers (2 cm for the TD-NIRS module, and 1.5 cm for the DCS module); which might guarantee a high sensitivity to thenar muscle.

Concerning baseline hemodynamic parameters reported in Sec. 3.1, the US measurements performed show that the superficial thicknesses of the four probed areas are lower than 5 mm for all subjects, suggesting that the interfiber distances used for these measurements (1.5 cm for DCS, and 2 cm for TD-NIRS) are sufficiently large to provide satisfactory sensitivity to muscle hemodynamics [32,75,76]. In this respect, no correlation was observed between hemodynamic parameters and thicknesses of superficial tissues. These results shall not be considered general, due to the particular population investigated (young and healthy people). The BFI, measured at 785 nm, was estimated considering the optical parameters (i.e., absorption and reduced scattering coefficients) measured at 830 nm. This approximation might influence the absolute values of BFI reported in Sec. 3.1. However, it does not affect the results shown for the PSDs, which were calculated from the relative variations of BFI.

Hemodynamic parameters measured in 14 healthy volunteers during resting state show larger variability, *i.e.*, standard deviation (particularly in case of  $S_tO_2$ , see Table 2) for thenar eminence compared to other muscles, probably due to the smaller dimension of the thenar muscle and the higher heterogeneity of the probed tissue. Indeed, even though its superficial thickness shows a lower inter-subject variability compared to other muscles (*e.g.*, forearm) [77], the proximity to bone, the small dimension of the muscle and its uneven shape could affect NIRS measurements. Indeed, except from thenar eminence,  $S_tO_2$  shows a coefficient of variation (CV, ratio between standard deviation and average value)  $< 6\%$ , in accordance with previous studies performed with a similar TD-NIRS device [78]. Despite this larger variability (which needs further investigation) VLF and LF components of BFI PSD are larger in the thenar eminence as compared to other muscles. This aspect together with the fact that thenar possesses a limited anatomical variability makes this muscle an excellent location for studying VLF and LF.

The reduced scattering and absorption coefficients measured on the four muscles are in accordance with previous works, in which optical properties of different skeletal muscles were measured [79,80]. The absorption coefficient and BFI are lower for the plantar fascia compared to the other muscles, probably because of the influence of the metatarsals bones (very proximal to the probe) [81] and the different type of tissue investigated which is actually an aponeurosis rather than true fascia, thus it can be considered a tendinous expansion, serving mainly to connect a muscle with the parts that it moves [82]. Lidner et al. [83] and Cortese et al. [84] measured the optical and dynamic properties of the sternocleidomastoid, and they reported lower values in terms of BFI and its standard deviation among subjects. However, they placed the probe in the proximity of the thyroid, whereas in our study DO measurements were performed on the extremity of the muscle, close to the jaw; moreover, they used a higher number of detection channels (15 at large distance) which lead to smaller standard errors [43].

## 5. Conclusions

In this work, we tested the possibility to assess LF and VLF spontaneous oscillations of microvasculature by resting state measurements of skeletal muscles hemodynamics via DO

methods. We measured 14 healthy subjects by simultaneous TD-NIRS and DCS measurements, on four different muscles (thenar eminence, plantar fascia, sternocleidomastoid and forearm) and reconstructing the PSDs of HHb, HbO<sub>2</sub>, tHb, S<sub>t</sub>O<sub>2</sub> and BFI during 15 min of resting state. Frequency analysis showed that TD-NIRS and DCS techniques are both suitable to detect VLF and LF oscillations. However, the PSD of BFI in VLF and LF bands was observed to be larger than the ones retrieved in PSDs of HHb, HbO<sub>2</sub>, tHb, S<sub>t</sub>O<sub>2</sub>. Concerning BFI, the PSD shows larger amplitude in distal muscles (thenar eminence and plantar fascia), suggesting that these muscles are more suitable to detect BFI oscillations compared to less distal muscles. According to previous literature on LDF and PPG, the peaks observed in PSD of BFI might be related to endothelium activities for VLF (*i.e.*, 0.0095-0.021 Hz) and neurogenic and myogenic activities at LF (*i.e.*, from 0.021 to 0.052 Hz and 0.052-0.145 Hz). Finally, as proof of principle, we measured the PSD of the hemodynamic parameters in a septic patient observing different behavior at myogenic frequencies compared to healthy subjects, in accordance with previous literature on LDF [71]. Moreover, lower PSDs at VLF were measured in all hemodynamic parameters of the septic patient compared to the ones of healthy subjects, that might suggest an impairment in endothelial functions. The present study paves the way for endothelium hemodynamic activity assessment in skeletal muscles via diffuse optical technologies with no need for other subsidiary intervention. Further studies can be done increasing the number of healthy volunteers and ICU patients, and exploiting more complex method of analysis (*e.g.*, wavelet transform), which might allow to compare the spectrum behavior during and after arterial occlusion with the nowadays more used parameters of deoxygenation and reoxygenation rate.

## 6. Appendix A

The statistical analysis performed on the absolute and relative PSD areas in the three intervals of interest are reported in the following tables.

**Table 4.** *p*-value computed by Wilcoxon signed-rank test comparing absolute areas of PSD for BFI in different regions of the body, in 14 healthy volunteers. In bold the statistically significant *p*-value according to Bonferroni correction for multiple comparisons.

		I <sub>1</sub> = [0.0095; 0.021] Hz			I <sub>2</sub> = [0.021; 0.052] Hz			I <sub>3</sub> = [0.052; 0.145] Hz		
		Plantar fascia	Sternoclei domastoid	Forearm	Plantar fascia	Sternoclei domastoid	Forearm	Plantar fascia	Sternoclei domastoid	Forearm
Absolute area	Thenar eminence	0.29	<b>0.001</b>	<b>0.0001</b>	0.50	<b>0.0003</b>	<b>0.0001</b>	0.76	<b>0.0002</b>	<b>0.0001</b>
	Plantar fascia	/	<b>0.0001</b>	<b>0.0001</b>	/	<b>0.0001</b>	<b>0.0001</b>	/	<b>0.0001</b>	<b>0.0008</b>
	Sternoclei domastoid	/	/	0.26	/	/	0.42	/	/	0.058

**Table 5. *p*-value computed by Wilcoxon signed-rank test comparing absolute and relative areas of PSD for HHb in different regions of the body, in 14 healthy volunteers. In bold the statistically significant *p*-value according to Bonferroni correction for multiple comparisons.**

		I <sub>1</sub> = [0.0095; 0.021] Hz			I <sub>2</sub> = [0.021; 0.052] Hz			I <sub>3</sub> = [0.052; 0.145] Hz		
		Plantar fascia	Sternoclei domastoid	Forearm	Plantar fascia	Sternoclei domastoid	Forearm	Plantar fascia	Sternoclei domastoid	Forearm
Absolute area	Thenar eminence	<b>0.0001</b>	0.13	<b>0.006</b>	<b>0.006</b>	0.049	0.53	<b>0.0002</b>	0.167	<b>0.008</b>
	Plantar fascia	/	<b>0.0001</b>	<b>0.0001</b>	/	<b>0.0008</b>	<b>0.0001</b>	/	<b>0.002</b>	<b>0.006</b>
	Sternoclei domastoid	/	/	0.07	/	/	0.453	/	/	0.261
Relative area	Thenar eminence	<b>0.0002</b>	0.98	0.013	0.040	0.491	0.572	<b>0.008</b>	0.03	0.03
	Plantar fascia	/	<b>0.0002</b>	<b>0.0001</b>	/	0.889	0.0476		<b>0.0001</b>	<b>0.0001</b>
	Sternoclei domastoid	/	/	0.03	/	/	0.1492			0.53

**Table 6. *p*-value computed by Wilcoxon signed-rank test comparing absolute and relative areas of PSD for HbO<sub>2</sub> in different regions of the body, in 14 healthy volunteers. In bold the statistically significant *p*-value according to Bonferroni correction for multiple comparisons.**

		I <sub>1</sub> = [0.0095; 0.021] Hz			I <sub>2</sub> = [0.021; 0.052] Hz			I <sub>3</sub> = [0.052; 0.145] Hz		
		Plantar fascia	Sternoclei domastoid	Forearm	Plantar fascia	Sternoclei domastoid	Forearm	Plantar fascia	Sternoclei domastoid	Forearm
Absolute area	Thenar eminence	<b>0.0001</b>	0.28	0.57	<b>0.0001</b>	<b>0.003</b>	<b>0.0001</b>	<b>0.0001</b>	<b>0.0002</b>	<b>0.0002</b>
	Plantar fascia	/	<b>0.0023</b>	<b>0.0003</b>	/	<b>0.015</b>	0.01	/	0.318	0.148
	Sternoclei domastoid	/	/	0.57	/	/	0.16	/	/	0.702
Relative area	Thenar eminence	<b>0.005</b>	0.167	<b>0.004</b>	0.937	0.131	0.288	0.048	0.491	0.703
	Plantar fascia	/	<b>0.0002</b>	<b>0.0006</b>	/	0.168	0.795	/	0.056	0.1689
	Sternoclei domastoid	/	/	0.61	/	/	0.319	/	/	0.261

**Table 7. *p*-value computed by Wilcoxon signed-rank test comparing absolute and relative areas of PSD for tHb in different regions of the body, in 14 healthy volunteers. In bold the statistically significant *p*-value according to Bonferroni correction for multiple comparisons.**

		I <sub>1</sub> = [0.0095; 0.021] Hz			I <sub>2</sub> = [0.021; 0.052] Hz			I <sub>3</sub> = [0.052; 0.145] Hz		
		Plantar fascia	Sternoclei domastoid	Forearm	Plantar fascia	Sternoclei domastoid	Forearm	Plantar fascia	Sternoclei domastoid	Forearm
Absolute area	Thenar eminence	0.012	<b>0.0012</b>	<b>0.0006</b>	<b>0.0001</b>	0.023	<b>0.0001</b>	<b>0.0001</b>	0.05	<b>0.0001</b>
	Plantar fascia	/	0.318	0.318	/	<b>0.0082</b>	0.040	/	<b>0.0038</b>	<b>0.101</b>
	Sternoclei domastoid	/	/	0.614	/	/	0.235	/	/	0.235
Relative area	Thenar eminence	<b>0.0023</b>	0.491	0.453	0.188	<b>0.0008</b>	0.020	0.288	<b>0.0006</b>	<b>0.003</b>
	Plantar fascia	/	0.131	<b>0.0039</b>	/	<b>0.0006</b>	<b>0.0052</b>	/	0.013	0.034
	Sternoclei domastoid	/	/	0.102	/	/	0.842	/	/	0.657

**Table 8.**  $p$ -value computed by Wilcoxon signed-rank test comparing absolute and relative areas of PSD for  $S_tO_2$  in different regions of the body, in 14 healthy volunteers. In bold the statistically significant  $p$ -value according to Bonferroni correction for multiple comparisons.

		$I_1 = [0.0095; 0.021]$ Hz			$I_2 = [0.021; 0.052]$ Hz			$I_3 = [0.052; 0.145]$ Hz		
		Plantar fascia	Sternoclei domastoid	Forearm	Plantar fascia	Sternoclei domastoid	Forearm	Plantar fascia	Sternoclei domastoid	Forearm
Absolute area	Thenar eminence	<b>0.0001</b>	0.843	0.657	<b>0.0001</b>	0.056	0.034	<b>0.0001</b>	<b>0.0001</b>	<b>0.0002</b>
	Plantar fascia	/	<b>0.0001</b>	<b>0.0002</b>	/	<b>0.008</b>	0.029	/	0.798	0.847
	Sternoclei domastoid	/	/	0.056	/	/	0.056	/	/	0.843
Relative area	Thenar eminence	<b>0.0002</b>	0.115	<b>0.006</b>	0.01	0.657	0.318	<b>0.005</b>	<b>0.0002</b>	<b>0.006</b>
	Plantar fascia	/	<b>0.0001</b>	<b>0.0002</b>	/	0.491	0.010	/	<b>0.006</b>	<b>0.0002</b>
	Sternoclei domastoid	/	/	0.065	/	/	0.168	/	/	0.417

## 7. Appendix B

In Table 9, we reported the median values and IRQ of PSD areas of hemodynamic parameters measured on healthy volunteers and on the septic patient, on the thenar eminence.

**Table 9.** Median and interquartile range of absolute and relative areas of PSD for hemodynamic parameters measured on the thenar eminence of healthy subjects, and same areas measured on the septic patient.

		$I_1 = [0.0095; 0.021]$ Hz			$I_2 = [0.021; 0.052]$ Hz			$I_3 = [0.052; 0.145]$ Hz		
		Median healthy	IQR healthy	Septic patient	Median healthy	IQR healthy	Septic patient	Median healthy	IQR healthy	Septic patient
Absolute area	HHb	0.137	0.046	0.016	0.049	0.019	0.013	0.093	0.028	0.049
	HbO <sub>2</sub>	0.094	0.044	0.009	0.088	0.016	0.034	0.156	0.049	0.082
	tHb	0.043	0.015	0.008	0.037	0.018	0.008	0.037	0.010	0.021
	$S_tO_2$	0.042	0.053	0.003	0.024	0.020	0.012	0.046	0.038	0.032
	BFI	24.469	44.642	6.702	32.092	42.477	18.572	19.297	25.526	26.157
Relative area	HHb	0.133	0.063	0.071	0.050	0.025	0.056	0.079	0.056	0.216
	HbO <sub>2</sub>	0.072	0.052	0.023	0.070	0.014	0.085	0.128	0.018	0.205
	tHb	0.161	0.061	0.067	0.121	0.028	0.071	0.144	0.0635	0.179
	$S_tO_2$	0.088	0.041	0.019	0.053	0.022	0.081	0.111	0.042	0.225
	BFI	0.218	0.070	0.084	0.257	0.071	0.232	0.184	0.099	0.327

**Funding.** European Social Fund; Secretaria d'Universitats i Recerca del Departament d'Empresa i Coneixement de la Generalitat de Catalunya; Fundació la Marató de TV3; Fundació Joan Ribas Araquistain; Generalitat de Catalunya; 'la Caixa' Foundation; The Severo Ochoa Center of Excellence; Agencia Estatal de Investigación; Ajuntament de Badalona; FUNDACIÓ Privada MIR-PUIG; Fundació Cellex; Ministero dell'Università e della Ricerca (2020477RW5PRIN); Marie Skłodowska-Curie (101062306); European Union's Horizon 2020 (101016087, 101017113, 675332, 688303, 871124).

**Acknowledgements.** This work has received funding from: the European Union's Horizon 2020 research and innovation programme under grant agreements No. 101016087 (VASCOVID), No. 101017113 (TINYBRAINS), No. 675332 (BITMAP), No. 688303 (LUCA), No. 871124 (LASERLAB-EUROPE V), the European Union's Horizon 2020 research and innovation programme under the Marie Skłodowska-Curie grant agreement No 101062306, Fundació CELLEX Barcelona, Fundació Mir-Puig, Ajuntament de Barcelona, Agencia Estatal de Investigación (PHOTOMETABO,

PID2019-106481RB-C31/10.13039/501100011033), the ‘‘Severo Ochoa’’ Programme for Centres of Excellence in R&D (CEX2019-000910-S), MEDLUX special program, the Obra social ‘‘la Caixa’’ Foundation (LlumMedBcn), Generalitat de Catalunya (CERCA, AGAUR-2022-SGR-01457, RIS3CAT-001-P-001682 CECH), Fundació Joan Ribas Araquistain (FJRA), Fundació La Marató de TV3. Additionally, this project has received funding from the Secretaria d’Universitats i Recerca del Departament d’Empresa i Coneixement de la Generalitat de Catalunya, as well as the European Social Fund (L’FSE inverteix en el teu futur)—FEDER.

This project is funded by MUR-PRIN2020, ‘‘Neuromuscular impairment in aging: a longitudinal study of structural and functional mechanistic bases of age-related alterations (Trajector-AGE)’’ grant number: 2020477RW5PRIN.

**Disclosures.** The role in the project of all the companies and their employees involved (pioNIRS s.r.l., ASPHALION S.L, BioPixs Ltd, HemoPhotonics S.L.) has been defined by the project objectives, tasks, and work packages and has been reviewed by the European Commission (European Union’s Horizon 2020 research and innovation programme, VASCOVID project, grant agreement No. 101016087).

ICFO has equity ownership in the spin-off company HemoPhotonics S.L. and UMW is the CEO. TD and UMW are inventors on relevant patents.

All the potential financial conflicts of interest and objectivity of research have been monitored by ICFO’s Knowledge & Technology Transfer Department. No financial conflicts of interest were identified.

M.B., M.L. A.T., A.T., and D.C. are cofounders of pioNIRS S.r.l., (Italy).

**Data availability.** Data underlying the results presented in this paper are not publicly available at this time but may be obtained from the authors upon reasonable request.

## References

1. E. V. Dolmatova, K. Wang, R. Mandavilli, and K. K. Griendling, ‘‘The effects of sepsis on endothelium and clinical implications,’’ *Cardiovasc. Res.* **117**(1), 60–73 (2021).
2. J. Duranteau, D. De Backer, K. Donadello, N. I. Shapiro, S. D. Hutchings, A. Rovas, M. Legrand, A. Harrois, and C. Ince, ‘‘The future of intensive care: the study of the microcirculation will help to guide our therapies,’’ *Crit. Care* **27**(1), 190 (2023).
3. M. Al-Qaisi, R. K. Kharbanda, T. K. Mittal, and A. E. Donald, ‘‘Measurement of endothelial function and its clinical utility for cardiovascular risk,’’ *Vasc. Health Risk Manage.* **4**, 647–652 (2008).
4. A. J. Flammer, T. Anderson, D. S. Celermajer, M. A. Creager, J. Deanfield, P. Ganz, N. M. Hamburg, T. F. Lüscher, M. Shechter, S. Taddei, J. A. Vita, and A. Lerman, ‘‘The assessment of endothelial function: From research into clinical practice,’’ *Circulation* **126**(6), 753–767 (2012).
5. B. Wu, D. Credeur, S. Fryer, and L. Stoner, ‘‘The use of shear rate-diameter dose-response curves as an alternative to the flow-mediated dilation test,’’ *Med. Hypotheses* **84**(2), 85–90 (2015).
6. L. Stoner, M. A. Tarrant, S. Fryer, and J. Faulkner, ‘‘How should flow-mediated dilation be normalized to its stimulus?’’ *Clin. Physiol. Funct. Imaging* **33**(1), 75–78 (2013).
7. F. Galetta, F. Franzoni, Y. Plantinga, L. Ghiadoni, M. Rossi, F. Prattichizzo, A. Carpi, S. Taddei, and G. Santoro, ‘‘Ambulatory blood pressure monitoring and endothelium-dependent vasodilation in the elderly athletes,’’ *Biomed. Pharmacother.* **60**(8), 443–447 (2006).
8. A. E. Donald, M. Charakida, T. J. Cole, P. Friberg, P. J. Chowieniczky, S. C. Millasseau, J. E. Deanfield, and J. P. Halcox, ‘‘Non-Invasive Assessment of Endothelial Function. Which Technique?’’ *J. Am. Coll. Cardiol.* **48**(9), 1846–1850 (2006).
9. A. Stefanovska and M. Bračič, ‘‘Physics of the human cardiovascular system,’’ *Contemp. Phys.* **40**(1), 31–55 (1999).
10. C. E. Thorn, H. Kyte, D. W. Slaff, and A. C. Shore, ‘‘An association between vasomotion and oxygen extraction,’’ *Am. J. Physiol. Hear. Circ. Physiol.* **301**(2), H442–H449 (2011).
11. P. Kvandal, S. A. Landsverk, A. Bernjak, A. Stefanovska, H. D. Kvernmo, and K. A. Kirkebøen, ‘‘Low-frequency oscillations of the laser Doppler perfusion signal in human skin,’’ *Microvasc. Res.* **72**(3), 120–127 (2006).
12. H. D. Kvernmo, A. Stefanovska, K. A. Kirkebøen, and K. Kvernebo, ‘‘Oscillations in the human cutaneous blood perfusion signal modified by endothelium-dependent and endothelium-independent vasodilators,’’ *Microvasc. Res.* **57**(3), 298–309 (1999).
13. S. J. Morris and A. C. Shore, ‘‘Skin blood flow responses to the iontophoresis of acetylcholine and sodium nitroprusside in man: Possible mechanisms,’’ *J. Physiol.* **496**(2), 531–542 (1996).
14. A. Schlez, M. Kittel, S. Braun, H. M. Häfner, and M. Jünger, ‘‘Endothelium-dependent regulation of cutaneous microcirculation in patients with systemic scleroderma,’’ *J. Invest. Dermatol.* **120**(2), 332–334 (2003).
15. H. D. Kvernmo, A. Stefanovska, and K. A. Kirkebøen, ‘‘Enhanced endothelial activity reflected in cutaneous blood flow oscillations of athletes,’’ *Eur. J. Appl. Physiol.* **90**(1-2), 16–22 (2003).
16. J. L. Cracowski, C. T. Minson, M. Salvat-Melis, and J. R. Halliwill, ‘‘Methodological issues in the assessment of skin microvascular endothelial function in humans,’’ *Trends Pharmacol. Sci.* **27**(9), 503–508 (2006).
17. J. Allen, ‘‘Photoplethysmography and its application in clinical physiological measurement,’’ *Physiol. Meas.* **28**(3), R1–R39 (2007).
18. M. A. Almarshad, M. S. Islam, S. Al-Ahmadi, and A. S. Bahammam, ‘‘Diagnostic Features and Potential Applications of PPG Signal in Healthcare: A Systematic Review,’’ *Healthc.* **10**(3), 547 (2022).



19. C. P. Anderson and S. Y. Park, "Assessing pulse transit time to the skeletal muscle microcirculation using near-infrared spectroscopy," *J. Appl. Physiol.* **133**(3), 593–605 (2022).
20. K. C. Doerschug, A. S. Delsing, G. A. Schmidt, and W. G. Haynes, "Impairments in microvascular reactivity are related to organ failure in human sepsis," *Am. J. Physiol. - Hear. Circ. Physiol.* **293**(2), H1065–H1071 (2007).
21. J. Mesquida, C. Espinal, G. Gruartmoner, J. Masip, C. Sabatier, F. Baigorri, M. R. Pinsky, and A. Artigas, "Prognostic implications of tissue oxygen saturation in human septic shock," *Intensive Care Med.* **38**(4), 592–597 (2012).
22. J. Mesquida, A. Caballer, L. Cortese, C. Vila, U. Karadeniz, M. Pagliuzzi, M. Zanoletti, A. Pérez Pacheco, P. Castro, M. García-de-Acilu, R. C. Mesquita, D. R. Busch, T. Durduran, and HEMOCOVID-19 Consortium, "Peripheral microcirculatory alterations are associated with the severity of acute respiratory distress syndrome in COVID-19 patients admitted to intermediate respiratory and intensive care units," *Crit. Care* **25**(1), 381 (2021).
23. J. Creteur, T. Carollo, G. Soldati, G. Buchele, D. De Backer, and J. L. Vincent, "The prognostic value of muscle StO<sub>2</sub> in septic patients," *Intensive Care Med.* **33**(9), 1549–1556 (2007).
24. D. Orbegozo Cortés, L. Rahmania, M. Irazabal, C. Santacruz, V. Fontana, D. De Backer, J. Creteur, and J. L. Vincent, "Microvascular reactivity is altered early in patients with acute respiratory distress syndrome," *Respir. Res.* **17**(1), 59 (2016).
25. L. Cortese, M. Zanoletti, U. Karadeniz, M. Pagliuzzi, M. A. Yaqub, D. R. Busch, J. Mesquida, and T. Durduran, "Performance assessment of a commercial continuous-wave near-infrared spectroscopy tissue oximeter for suitability for use in an international, multi-center clinical trial," *Sensors* **21**(21), 6957 (2021).
26. M. Lipcsey, N. C. Z. Woinarski, and R. Bellomo, "Near infrared spectroscopy (NIRS) of the thenar eminence in anesthesia and intensive care," *Ann. Intensive Care* **2**(1), 11 (2012).
27. H. Gómez, A. Torres, P. Polanco, H. K. Kim, S. Zenker, J. C. Puyana, and M. R. Pinsky, "Use of non-invasive NIRS during a vascular occlusion test to assess dynamic tissue O<sub>2</sub> saturation response," *Intensive Care Med.* **34**(9), 1600–1607 (2008).
28. G. Gruartmoner, J. Mesquida, and C. Ince, "Microcirculatory monitoring in septic patients: Where do we stand?" *Med. Intensiva* **41**(1), 44–52 (2017).
29. J. Selb, M. A. Yücel, D. Phillip, H. W. Schytz, H. K. Iversen, M. Vangel, M. Ashina, and D. A. Boas, "Effect of motion artifacts and their correction on near-infrared spectroscopy oscillation data: a study in healthy subjects and stroke patients," *J. Biomed. Opt.* **20**(5), 056011 (2015).
30. L. Couch, M. Roskosky, B. A. Freedman, and M. S. Shuler, "Effect of Skin Pigmentation on Near Infrared Spectroscopy," *Am. J. Anal. Chem.* **06**(12), 911–916 (2015).
31. . "VASCOVID European project (Horizon 2020)," <https://vascovid.eu/>.
32. A. Torricelli, D. Contini, A. Pifferi, M. Caffini, R. Re, L. Zucchelli, and L. Spinelli, "Time domain functional NIRS imaging for human brain mapping," *NeuroImage* **85**, 28–50 (2014).
33. T. Durduran and A. G. Yodh, "Diffuse correlation spectroscopy for non-invasive, micro-vascular cerebral blood flow measurement," *NeuroImage* **85**, 51–63 (2014).
34. C. Amendola, M. Lacerenza, M. Buttafava, A. Tosi, L. Spinelli, D. Contini, and A. Torricelli, "A compact multi-distance dcs and time domain nirs hybrid system for hemodynamic and metabolic measurements," *Sensors* **21**(3), 870 (2021).
35. H. Obrig, M. Neufang, R. Wenzel, M. Kohl, J. Steinbrink, K. Einhäupl, and A. Villringer, "Spontaneous low frequency oscillations of cerebral hemodynamics and metabolism in human adults," *NeuroImage* **12**(6), 623 (2000).
36. A. V. Andersen, S. A. Simonsen, H. W. Schytz, and H. K. Iversen, "Assessing low-frequency oscillations in cerebrovascular diseases and related conditions with near-infrared spectroscopy: a plausible method for evaluating cerebral autoregulation?" *Neurophotonics* **5**(03), 1 (2018).
37. Z. Zhang and R. Khatami, "Predominant endothelial vasomotor activity during human sleep: A near-infrared spectroscopy study," *Eur. J. Neurosci.* **40**(9), 3396–3404 (2014).
38. Q. Tan, Y. Wang, Z. Li, D. Wang, W. K. Lam, D. W. C. Wong, Y. Peng, G. Zhang, and M. Zhang, "Spectral analysis of muscle hemodynamic responses in post-exercise recovery based on near-infrared spectroscopy," *Sensors* **21**(9), 3072 (2021).
39. T. Y. Lin, L. L. Lin, T. C. Ho, and J. J. J. Chen, "Investigating the adaptation of muscle oxygenation to resistance training for elders and young men using near-infrared spectroscopy," *Eur. J. Appl. Physiol.* **114**(1), 187–196 (2014).
40. Q. Tan, Y. Wang, T. L. W. Chen, D. W. C. Wong, F. Yan, Z. Li, and M. Zhang, "Exercise-induced hemodynamic changes in muscle tissue: Implication of muscle fatigue," *Appl. Sci.* **10**(10), 3512 (2020).
41. C. Yeo, H. Jung, K. Lee, and C. Song, "Low frequency oscillations assessed by diffuse speckle contrast analysis for foot angiosome concept," *Sci. Rep.* **10**(1), 17153 (2020).
42. M. Lacerenza, M. Buttafava, M. Renna, A. Dalla Mora, L. Spinelli, F. Zappa, A. Pifferi, A. Torricelli, A. Tosi, and D. Contini, "Wearable and wireless time-domain near-infrared spectroscopy system for brain and muscle hemodynamic monitoring," *Biomed. Opt. Express* **11**(10), 5934–5949 (2020).
43. L. Cortese, G. Lo Presti, M. Pagliuzzi, D. Contini, A. Dalla Mora, H. Dehghani, F. Ferri, J. B. Fischer, M. Giovannella, F. Martelli, U. M. Weigel, S. Wojtkiewicz, M. Zanoletti, and T. Durduran, "Recipes for diffuse correlation spectroscopy instrument design using commonly utilized hardware based on targets for signal-to-noise ratio and precision," *Biomed. Opt. Express* **12**(6), 3265–3281 (2021).

44. C. Amendola, M. Lacerenza, I. Pirovano, D. Contini, L. Spinelli, R. Cubeddu, A. Torricelli, and R. Re, "Optical characterization of 3D printed PLA and ABS filaments for diffuse optics applications," *PLoS One* **16**(6), e0253181 (2021).
45. M. Zanoletti, L. Cortese, and C. Amendola, *et al.*, "VASCOVID: An integrated platform to evaluate endothelial and microvascular impairment in severe COVID-19 patients," in *Optics InfoBase Conference Papers* (2021), p. ETh3A.4.
46. T. J. Farrell, M. S. Patterson, and B. Wilson, "A Diffusion Theory Model of Spatially Resolved, Steady-State Diffuse Reflectance for the Noninvasive Determination of Tissue Optical Properties in Vivo," *Med. Phys.* **19**(4), 879–888 (1992).
47. R. C. Haskell, L. O. Svaasand, T.-T. Tsay, T.-C. Feng, M. S. McAdams, and B. J. Tromberg, "Boundary conditions for the diffusion equation in radiative transfer," *J. Opt. Soc. Am. A* **11**(10), 2727–2741 (1994).
48. K. Levenberg, "A method for the solution of certain non-linear problems in least squares," *Q. Appl. Math.* **2**(2), 164–168 (1944).
49. B. J. Ackerson, R. L. Dougherty, N. M. Reguigui, and U. Nobbmann, "Correlation transfer: Application of radiative transfer solution methods to photon correlation problems," *J. Thermophys. Heat Transf.* **6**(4), 577–588 (1992).
50. D. A. Boas and A. G. Yodh, "Spatially varying dynamical properties of turbid media probed with diffusing temporal light correlation," *J. Opt. Soc. Am. A* **14**(1), 192–215 (1997).
51. J. C. Lagarias, J. A. Reeds, M. H. Wright, and P. E. Wright, "Convergence properties of the Nelder-Mead simplex method in low dimensions," *SIAM J. Optim.* **9**(1), 112–147 (1998).
52. R. Cheng, Y. Shang, D. Hayes, S. P. Saha, and G. Yu, "Noninvasive optical evaluation of spontaneous low frequency oscillations in cerebral hemodynamics," *NeuroImage* **62**(3), 1445–1454 (2012).
53. H. Cheng, J. Yu, L. Xu, and J. Li, "Power spectrum of spontaneous cerebral hemodynamic oscillation shows a distinct pattern in autism spectrum disorder," *Biomed. Opt. Express* **10**(3), 1383–1392 (2019).
54. J. Mesquida, G. Gruartmoner, C. Espinal, J. Masip, C. Sabatier, A. Villagrà, H. Gómez, M. Pinsky, F. Baigorri, and A. Artigas, "Thenar oxygen saturation (StO<sub>2</sub>) alterations during a spontaneous breathing trial predict extubation failure," *Ann. Intensive Care* **10**(1), 54 (2020).
55. J. Mesquida, G. Gruartmoner, and C. Espinal, "Skeletal muscle oxygen saturation (StO<sub>2</sub>) measured by near-infrared spectroscopy in the critically ill patients," *Biomed Res. Int.* **2013**, 1–8 (2013).
56. I. Mizeva, C. Di Maria, P. Frick, S. Podtaev, and J. Allen, "Quantifying the correlation between photoplethysmography and laser Doppler flowmetry microvascular low-frequency oscillations," *J. Biomed. Opt.* **20**(3), 037007 (2015).
57. K. Ažman-Juvan, A. Bernjak, V. Urbančič-Rovan, A. Stefanovska, and D. Štajer, "Skin blood flow and its oscillatory components in patients with acute myocardial infarction," *J. Vasc. Res.* **45**(2), 164–172 (2008).
58. P. Kvandal, A. Stefanovska, M. Veber, H. D. Kvermmo, and K. A. Kirkeboen, "Regulation of human cutaneous circulation evaluated by laser Doppler flowmetry, iontophoresis, and spectral analysis: Importance of nitric oxide and prostaglandines," *Microvasc. Res.* **65**(3), 160–171 (2003).
59. A. Stefanovska, M. Bracic, and H. D. Kvermmo, "Wavelet analysis of oscillations in the peripheral blood circulation measured by laser Doppler technique," *IEEE Trans. Biomed. Eng.* **46**(10), 1230–1239 (1999).
60. J. Kastrop, J. Bülow, and N. A. Lassen, "Vasomotion in human skin before and after local heating recorded with laser Doppler flowmetry. A method for induction of vasomotion," *Int. J. Microcirc. Clin. Exp.* **8**, 205 (1989).
61. S. A. Landsverk, P. Kvandal, T. Kjelstrup, U. Benko, A. Bernjak, A. Stefanovska, H. Kvermmo, and K. A. Kirkeboen, "Human skin microcirculation after brachial plexus block evaluated by wavelet transform of the laser doppler flowmetry signal," *Anesthesiology* **105**(3), 478–484 (2006).
62. J. Mesquida, G. Gruartmoner, M. L. Martínez, J. Masip, C. Sabatier, C. Espinal, A. Artigas, and F. Baigorri, "Thenar oxygen saturation and invasive oxygen delivery measurements in critically ill patients in early septic shock," *Shock* **35**(5), 456–459 (2011).
63. H. D. Kvermmo, A. Stefanovska, M. Bracic, K. A. Kirkeboen, and K. Kvernebo, "Spectral analysis of the laser Doppler perfusion signal in human skin before and after exercise," *Microvasc. Res.* **56**(3), 173–182 (1998).
64. T. Söderström, A. Stefanovska, M. Veber, and H. Svensson, "Involvement of sympathetic nerve activity in skin blood flow oscillations in humans," *Am. J. Physiol. - Hear. Circ. Physiol.* **284**(5), H1638–H1646 (2003).
65. W. M. Bayliss, "On the local reactions of the arterial wall to changes of internal pressure," *J. Physiol.* **28**(3), 220–231 (1902).
66. S. A. Landsverk, P. Kvandal, A. Bernjak, A. Stefanovska, and K. A. Kirkeboen, "The effects of general anesthesia on human skin microcirculation evaluated by wavelet transform," *Anesth. Analg.* **105**(4), 1012–1019 (2007).
67. W. F. Jackson, "Myogenic Tone in Peripheral Resistance Arteries and Arterioles: The Pressure Is On!" *Front. Physiol.* **12**, 699517 (2021).
68. J. C. Falcone, M. J. Davis, and G. A. Meininger, "Endothelial independence of myogenic response in isolated skeletal muscle arterioles," *Am. J. Physiol.* **260**(1), H130–H135 (1991).
69. J. Přibíl, A. Přibílová, and I. Frollo, "Comparative Measurement of the PPG Signal on Different Human Body Positions by Sensors Working in Reflection and Transmission Modes †," *Eng. Proc.* **2**, 69 (2020).
70. T. Yano, C. S. Lian, R. Afroundeh, K. Shirakawa, and T. Yunoki, "Comparison of oscillations of skin blood flow and deoxygenation in vastus lateralis in light exercise," *Biol. Sport* **31**(1), 15–20 (2013).
71. J. D. Young and E. M. Cameron, "Dynamics of skin blood flow in human sepsis," *Intensive Care Med.* **21**(8), 669–674 (1995).

72. J. Joffre and J. Hellman, "Oxidative stress and endothelial dysfunction in sepsis and acute inflammation," *Antioxidants Redox Signal.* **35**(15), 1291–1307 (2021).
73. D. P. Jayawardena, N. P. Kulkarni, and S. E. Gill, "The role of tissue inhibitors of metalloproteinases in microvascular endothelial cell barrier dysfunction during sepsis," *Met. Med.* **6**, 1–12 (2019).
74. M. Giovannella, E. Urtane, M. Zanoletti, U. Karadeniz, U. Rubins, U. M. Weigel, Z. Marcinkevics, and T. Durduran, "Microvascular blood flow changes of the abductor pollicis brevis muscle during sustained static exercise," *Biomed. Opt. Express* **12**(7), 4235 (2021).
75. I. Pirovano, S. Porcelli, R. Re, L. Spinelli, D. Contini, M. Marzorati, and A. Torricelli, "Effect of adipose tissue thickness and tissue optical properties on the differential pathlength factor estimation for NIRS studies on human skeletal muscle," *Biomed. Opt. Express* **12**(1), 571–587 (2021).
76. R. Istfan, C. A. Gómez, M. Applegate, D. Rozenberg, W. D. Reid, and D. Roblyer, "Hemodynamics of the sternocleidomastoid measured with frequency domain near-infrared spectroscopy towards non-invasive monitoring during mechanical ventilation," *Biomed. Opt. Express* **12**(7), 4147–4162 (2021).
77. M. Poeze, "Tissue-oxygenation assessment using near-infrared spectroscopy during severe sepsis: Confounding effects of tissue edema on StO<sub>2</sub> values," *Intensive Care Med.* **32**(5), 788–789 (2006).
78. B. Andresen, A. De Carli, M. Fumagalli, M. Giovannella, T. Durduran, U. Michael Weigel, D. Contini, L. Spinelli, A. Torricelli, and G. Greisen, "Cerebral oxygenation and blood flow in normal term infants at rest measured by a hybrid near-infrared device (BabyLux)," *Pediatr. Res.* **86**(4), 515–521 (2019).
79. A. Torricelli, V. Quaresima, A. Pifferi, G. Biscotti, L. Spinelli, P. Taroni, M. Ferrari, and R. Cubeddu, "Mapping of calf muscle oxygenation and haemoglobin content during dynamic plantar flexion exercise by multi-channel time-resolved near-infrared spectroscopy," *Phys. Med. Biol.* **49**(5), 685–699 (2004).
80. A. N. Bashkatov, E. A. Genina, V. I. Kochubey, and V. V. Tuchin, "Optical properties of human cranial bone in the spectral range from 800 to 2000nm," in *Proc. SPIE 6163, Saratov Fall Meeting 2005: Optical Technologies in Biophysics and Medicine VII*, 616310 (2006), p. 616310.
81. S. Konugolu Venkata Sekar, M. Pagliazzi, E. Negro, F. Martelli, A. Farina, A. Dalla Mora, C. Lindner, P. Farzam, N. Pérez-Álvarez, J. Puig, P. Taroni, A. Pifferi, and T. Durduran, "In Vivo, non-invasive characterization of human bone by hybrid broadband (600-1200 nm) diffuse optical and correlation spectroscopies," *PLoS One* **11**(12), e0168426 (2016).
82. M. R. Hedrick, "The plantar aponeurosis," *Foot Ankle Int.* **17**(10), 646–649 (1996).
83. C. Lindner, M. Mora, P. Farzam, M. Squarcia, J. Johansson, U. M. Weigel, I. Halperin, F. A. Hanzu, and T. Durduran, "Diffuse optical characterization of the healthy human thyroid tissue and two pathological case studies," *PLoS One* **11**(1), e0147851 (2016).
84. L. Cortese, P. Fernández Esteberena, and M. Zanoletti, *et al.*, "In vivo characterization of the optical and hemodynamic properties of the human sternocleidomastoid muscle through ultrasound-guided hybrid near-infrared," *bioRxiv*, (2023).